Materials Chemistry and Physics 205 (2018) 303–314

Contents lists available at ScienceDirect

Materials Chemistry and Physics

journal homepage: www.elsevier.com/locate/matchemphys

Effect of amine modification on morphology and performance of poly (ether-block-amide)/fumed silica nanocomposite membranes for CO_2/CH_4 separation

Mojgan Isanejad, Toraj Mohammadi*

Research and Technology Center of Membrane Processes, Faculty of Engineering Department, Iran University of Science and Technology (IUST), Narmak, Tehran, Iran

HIGHLIGHTS

- Amine functionalization of fumed silica nanoparticles was investigated.
- Novel modified fumed silica was used as filler.
- PEBAX1657/Silica nanocomposite membranes were developed.
- An experimental separation study of CO_2 using nanocomposite membranes was proposed.
- Effect of SiO_2 loading, feed pressure & temperature on gas separation was studied.

GRAPHICAL ABSTRACT

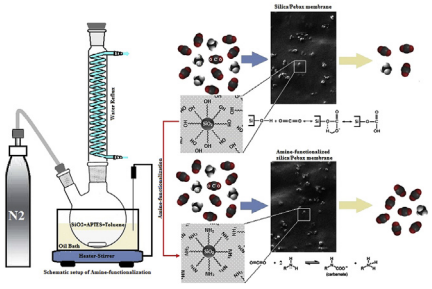

ARTICLE INFO

Article history:
Received 10 May 2017
Received in revised form
6 November 2017
Accepted 10 November 2017
Available online 13 November 2017

Keywords:
PEBAX
CO_2/CH_4 separation
Fumed silica
Surface modification

ABSTRACT

In this study, fumed silica nanoparticles were functionalized using amine groups and used as inorganic modifiers for preparation of poly (ether-block-amide) based nanocomposite membranes. Field-emission scanning electron microscopy (FESEM), X-ray diffraction (XRD), Fourier-transform infrared spectroscopy (FTIR) and CHNO elemental analysis were used to characterize nanoparticles and nanocomposite membranes. The prepared membranes were applied for separation of carbon dioxide (CO_2) from methane (CH_4). The effects of nanoparticles loading, feed pressure and feed temperature on permeability and CO_2/CH_4 ideal selectivity of the nanocomposite membranes were investigated. The results indicated that addition of 15 wt % of amine-functionalized fumed silica nanoparticles in the casting solution enhances the membrane CO_2 permeability and CO_2/CH_4 ideal selectivity 10% and 14%, respectively.

1. Introduction

Carbon dioxide (CO_2) is one of the most important acid gases in natural gas and many other gas streams [1,2]. Presence of CO_2 in natural-gas streams leads to several serious problems such as pipeline and equipment corrosion and reduction of natural-gas heating value and pipeline capacity [3–5]. Traditional processes for CO_2 capturing are based on reversible chemical or physical absorption or adsorption such as amine scrubbing and cryogenic distillation, but these processes are high energy-consuming in terms of solvent regeneration and equipment corrosion [3,6,7]. Many gas separation tasks, especially natural-gas purification, need more economically and environmentally new efficient separation processes such as fast improving and spreading membrane processes [6,8–11]. Compared to traditional CO_2 separation processes,

* Corresponding author.
E-mail address: torajmohammadi@iust.ac.ir (T. Mohammadi).

https://doi.org/10.1016/j.matchemphys.2017.11.018
0254-0584/

polymer-based membrane processes have several advantages, including low capital cost, low energy consumption, low maintenance operations, high flexibility, small footprints and exceptional reliability, which have given these processes a great potential for CO_2 capturing [12–16].

Glassy polyamides (PA) have been widely used in gas separation membranes due to their rigid and selective nature. In contrast, rubbery polyethers (PE) due to the flexible chains and the presence of voids, contain large free volume [17]. Poly (ether-block-amide) resin known as the trademark PEBAX® is a thermoplastic elastomer having both hard rigid PA segments which give mechanical strength, and soft flexible-chain PE segments that offer high permeability. Commercially various grades of PEBAX® copolymers are available by different ether and amide ratios [17–19]. PEBAX® copolymers due to their desirable properties such as mechanical strength and thermal resistance, high durability, flexibility and favorable selectivity have been extensively used for acid gas treatment and separation of polar/non-polar gases, i.e. CO_2/CH_4 [20,21].

Although polymeric membranes, like PEBAX®, have outstanding separation performance, they generally undergo the Robeson upper bound curves, a trade-off limitation between permeability and selectivity. Membranes with separation performances above this limit are attractive for industrial applications. Thus, there is an increasing demand to improve the membrane performance, i.e. permeability and selectivity by modifying the polymeric matrix [14,22–24]. Incorporation of a second phase such as a polymeric phase [25] or inorganic nanoparticles into the polymeric matrix is among the recent polymeric membrane development strategies. Nanocomposite membranes are simultaneous combination of processability and flexibility of polymers with selectivity, thermal and mechanical stability of nanoparticles, which possibly develop new synergistic properties [18,20,26].

Various types of inorganic modifiers, including nonporous particles such as SiO_2 [27] and TiO_2 [28] and porous particles like zeolites [29], metal organic frameworks (MOFs) [13] and multi-walled carbon nanotubes (MWCNTs) [30] have been used to fabricate composite membranes. Among them, SiO_2 and its derivatives due to their high mechanical and thermal stabilities, high specific surface area and the ability of chemical functionalization are proved to be promising modifiers for gas separation membranes [31–33]. Modifier chemical functionalization with groups such as amines, is a method to improve nanoparticles separation performance and their dispersion into the polymer matrix [13,26,34].

In this paper, amine-functionalized SiO_2 nanoparticles were prepared and used as a modifier to enhance the performance of PEBAX® membrane. Amine has been proved as an effective group in achieving high CO_2 permeability and CO_2/CH_4 ideal selectivity. Physical and chemical properties of amine-functionalized SiO_2/PEBAX® 1657 nanocomposite membranes were characterized. Preparation and operation parameters, including modifier loading, feed temperature and feed pressure were investigated and permeability and CO_2/CH_4 ideal selectivity of the prepared nanocomposite membranes were measured.

2. Experimental

2.1. Materials

Pebax-1657, a thermoplastic elastomer consists of rigid PA segments separated by flexible PE segments, that contains 60 wt % of poly (ethylene oxide) (PEO) and 40 wt % polyamide 6 (PA-6) was supplied by Arkema Inc. [21]. Methanol, n-Hexane and Toluene were supplied by Merck. N, N-Dimethyl Formamide (DMF) and (3-Aminopropyl) triethoxysilane (APTES) both in 99.99% purity were purchased from ROYALEX® and Sigma-Aldrich, respectively. Hydrophilic fumed silica nanoparticles with an average diameter of 40 nm and specific surface area of 50 ± 15 m^2/g was provided by AEROSIL®. The CO_2 and CH_4 gases (purity 99.99%) for permeation tests and N_2 gas for functionalization procedure were supplied from Oxygen Sablan (Tehran, Iran).

2.2. Amine functionalization of nanoparticles

Amine modification of silica nanoparticles before being loaded into the polymer matrix was performed, in order to enhance separation properties of PEBAX/Silica nanocomposite membranes by increasing surface interactions with CO_2 molecules. APTES, with the chemical structure as shown in Fig. 1, was used as a coupling agent between the polymer and modifier, in addition to interacting with polar gas molecules. In order to graft aminopropyl chains of this reagent to the surface of silica nanoparticles, it is necessary to first hydrolyze the ethoxy groups [35]. The hydrolysis procedure was performed using acidic water (pH = 2) in an organic medium (methanol) with molar ratios of 2 and 3 to the APTES content, respectively. Acidic water was added to the APTES-methanol solution dropwise under vigorous stirring. After 6 h aging, the solution was ready to be used in the functionalization process of the nanoparticles. To carry out the functionalization process, 5 g of nonporous SiO_2 was dispersed uniformly in 120 ml anhydrous toluene using an ultrasonic homogenizer. The hydrolyzed APTES was then added to the solution, and the mixture was stirred overnight at the reflux temperature under N_2 atmosphere. The amine functionalized silica nanoparticles (AFS) was then washed with ethanol and isolated by centrifugation/redispersion process (3X, 15 min, 12000 rpm). The mechanism of functionalization process is presented in Fig. 1.

2.3. Membranes preparation

The 6 wt % polymeric solution was prepared by dissolving 0.471 g of the polymer PEBAX 1657 in 7.379 g of DMF. DMF was selected due to close solubility parameter to the polymer's and its lower boiling point, which moderates operational conditions of preparation and drying processes and the prepared membranes

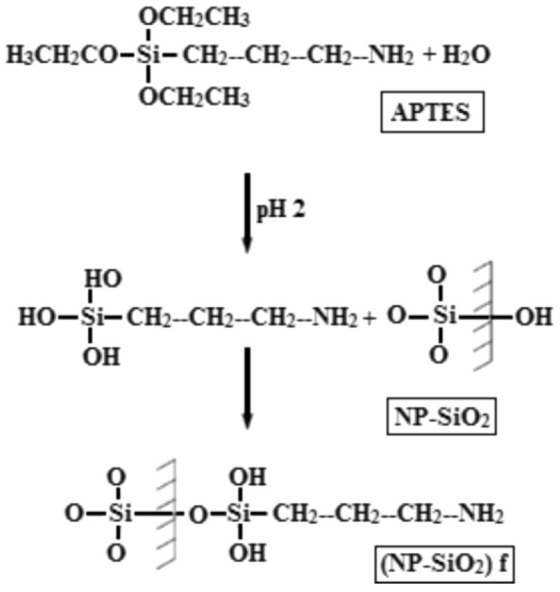

Fig. 1. Amine functionalization mechanism of SiO_2 nanoparticles [39].

were more uniform [36,37]. Furthermore, another considerable reason for application of DMF was that it causes gelation of the polymeric solution while coming out of oil bath and staying at ambient temperature. This prevents the nanoparticles in the polymeric film from sedimentation and agglomeration during the drying process. The intended nanoparticles were added to the solvent in levels of 0–20 wt % using the ID code of S-X for silica and AFS-X for amine functionalized silica incorporated membranes (X demonstrates the nanoparticles loading) and sonicated for 20 min before dissolving the polymer in the solvent, in order to be uniformly dispersed in the membrane. The polymer-nanoparticles solutions were then heated in an oil bath at 125 °C for 3 h under reflux and magnetic stirring. Finally, the obtained solutions were filtrated and via the solution-casting method, they were cast on petri dishes and dried at 50 °C overnight. After complete evaporation of the solvent, the prepared membranes were peeled off using hexane as non-solvent and treated overnight at 50 °C under vacuum to remove any residual gases and guest molecules before any further applications. All the raw materials were dried overnight at 70 °C under vacuum, prior to use. All the membranes were prepared with the average thickness of 65 μm.

2.4. Characterization

Fourier-transform-infrared spectroscopy (FTIR) was performed using an FTIR spectrometer Perkin–Elmer (Waltham, MA, USA) Spectrum RX1 in the range of 400–4400 cm^{-1} to investigate the functional groups and determine any changes in chemical composition of the prepared membranes and modified nanoparticles during the preparation processes.

Morphology and nanoparticles' dispersion for the prepared nanocomposite membranes were investigated using a Field-emission scanning electron microscope (FESEM) of Sigma, Zeiss. To clearly observe a cross-section of the membranes, the samples were fractured cryogenically in liquid nitrogen and subsequently top-coated with Au under vacuum condition.

X-ray diffraction (XRD) analysis was performed with an INEL model EQUINOX 3000, France X-ray diffractometer using Cu Kα X radiation with a wavelength of 1.5406° over the angle (2θ) range of 5°–75° at the scan rate of 0.01° s^{-1} to examine crystallinity of the membranes and nanoparticles. Patterns analysis and calculations of related data were performed by X'Pert HighScore and OriginPro 2016.

CHNO analysis was carried out using a Costec, ECS 4010 to determine the number of amine sites in a certain amount of modified nanoparticles using percentages of C, H and N elements in the samples.

For quantification of active amine sites in the amine functionalized samples and to calculate the efficiency of functionalization, back titration was carried out [38].

2.5. Gas permeation tests

The gas permeability of the membranes was examined using a constant volume setup in a pressure range of 2–10 bar for CO_2 and CH_4. The test setup is made of two compartment stainless steel cells in a way that a flat circular membrane with an effective area of 10.45 cm^2, and a reticular steel support were placed between two flanges and held by O-rings to avoid gas leakage. Before using the gases as feed, all the experiments were started by evacuating the cell up to −0.1 bar using a vacuum pump for driving out any residual gases from the cell to avoid further measurement errors. By using the constant volume method, the rate of permeation in Barrer (1 Barrer = 1×10^{-10} cm^3 (STP)-cm/cm^2 s cmHg) was calculated from the changes in pressure on the permeate side (with a known volume) versus time, according to the following equation:

$$P = \frac{273 \times 10^{10}}{760} \frac{VL}{AT\left(\frac{p_2 \times 76}{14.7}\right)} \left(\frac{dp}{dt}\right) \quad (1)$$

In which V refers to the volume of the permeate side in cm^3, L and A represent membrane thickness and the effective area in cm and cm^2, respectively and T is the absolute temperature. P_2 is the feed pressure of the upstream in bar and $\frac{dp}{dt}$ is the slope of permeate pressure change versus time, in its steady state (linear) region. Permeability data of two gases were measured for 3 membranes of each sample, and the average values were reported considering the error bars. The CO_2/CH_4 ideal selectivity (α_{CO_2/CH_4}) of the membranes was determined as the ratio of CO_2 permeance ($(P/l)_{CO_2}$) to CH_4 permeance ($(P/l)_{CH_4}$), using the following equation:

$$\alpha_{CO_2/CH_4} = \frac{(P/l)_{CO_2}}{(P/l)_{CH_4}} \quad (2)$$

2.6. Gas adsorption measurements

Isothermal adsorptions of CO_2 and CH_4 gases on fumed silica nanoparticles were measured via the pressure decay method in a constant-volume cell. The neat and amine functionalized silica nanoparticles were examined at 25 °C in the pressure range of 3–10 bar. In order to measure pressure changes during the adsorption process, a DMP 343 BD transmitter of 1 mbar accuracy was utilized and the output data were displayed and recorded by NX v.1.0.0. Before every experiment, the nanoparticles samples were treated for 24 h at 150 °C under vacuum to remove excess moisture and unwanted adsorbed gases. To perform the experiments, a certain amount of the activated nanoparticles was placed in the adsorption cell. The cell was totally evacuated and then filled by the gas up to the certain pressure by a sudden pulse. The adsorbed amount of gas molecules on the nanoparticles was obtained using the pressure decline and converted to the adsorbed moles of gas by the Peng-Robinson equation of state, as the most accurate EOS for the thermodynamic system of this work. Since the adsorption process was extremely sensitive to the temperature changes, it was kept constant during the experiments by a temperature control vessel with an accuracy of ±2 K.

3. Results and discussion

3.1. Characterization

3.1.1. FTIR analysis

Amine functionalized silica nanoparticles and the prepared membranes were characterized using Fourier-transform infrared spectroscopy (FTIR), as displayed in Fig. 2. The specific peaks of APTES reagent dedicated to amine functional groups are N-H bending vibration for the primary amine at 1575 cm^{-1} and 771 cm^{-1}, as shown in Fig. 2 (a). The weak stretching band in the range of 3300–3500 cm^{-1} correlates to NH_2 group. In comparison with silica nanoparticles spectrum, all the described peaks of APTES reagent appeare in the spectrum of amine functionalized silica, except NH_2 peaks which overlap the intense peak of abundant silanol groups of the surface (in the range of 3300–3600 cm^{-1}) and are not recognizable easily, but the reduce in OH peak intensity in Fig. 2 (c) is a sign of replacing these groups with amine groups. Moreover, the Si-O-Si characteristic peak of silica at 1110 cm^{-1} shows the increased intensity compared to Fig. 2 (b), due to the grafting of the aminosilane groups on the surface containing Si-O bonds inside [27,39].

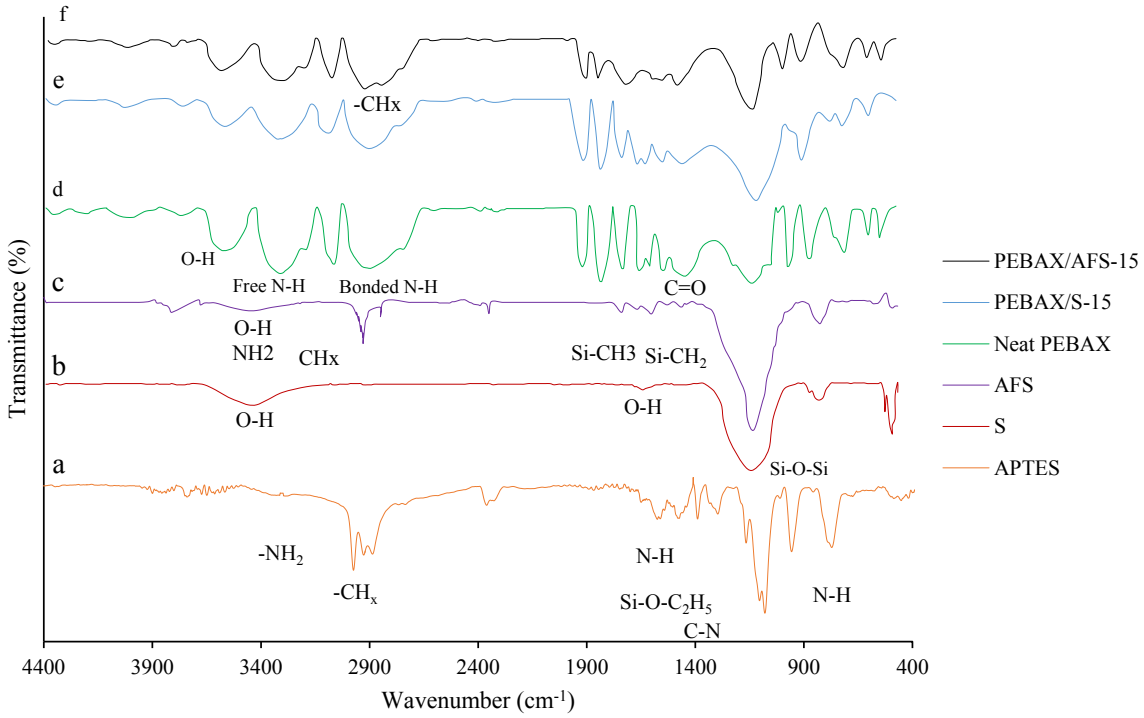

Fig. 2. FTIR spectra of a) APTES and b) SiO_2 and c) SiO_2-NH_2 nanoparticles and d) neat PEBAX, e) PEBAX/S-15 and f) PEBAX/AFS-15 membranes.

Since the silica and amine functionalized silica nanoparticles were loaded into PEBAX matrix, FTIR spectra of the 15 wt % loaded nanocomposite membranes represent some changes in the polymer characteristic peaks, in comparison with that of the pristine PEBAX 1657 membrane. For the neat membrane, the aliphatic −C−H stretching is revealed by the sharp band at around 2904 cm^{-1} and the peaks at 1730 cm^{-1} and 3312 cm^{-1} are dedicated to −C=O and −N−H stretching vibrations, respectively [40]. The broad peak at 3400-3700 cm^{-1} correlates to O−H groups, which represents the hydrogen bonding between hard segments of the polymer chains.

Incorporation of the neat and modified nanoparticles causes some changes in position and intensity of polymer characteristic peaks in the IR spectra, due to the polymer-nanoparticles interactions. In the range of 900–1400 cm^{-1}, the effect of the Si-O-Si broad peak of the nanoparticles in the polymer matrix is clearly observed in both nanocomposites spectra of Fig. 2 (e, f). It is obvious that some characteristic peaks of the PEBAX membrane are reduced in intensity and shifted left towards higher frequencies due to the presence of nanoparticles. This suggests that the incorporation of the silica nanoparticles in the polymer matrix partially breaks hydrogen bonding between amide nitrogen of PA segments with each other or with the carbonyl oxygen of other chains, which are associated with the polymer chains and induced a microcrystalline structure [41]. Therefore, as observed in Fig. 2 (e), N−H stretching vibration of the polymer's amide group, consists of two peaks at 3312 cm^{-1} and 3202 cm^{-1} that are ascribed to free and hydrogen bonded N−H groups, respectively. In the presence of silica nanoparticles, a considerable reduction in intensities is observed for both peaks and the hydrogen-bonded peak shifts from 3202 to 3207 cm^{-1}, due to partial disruption of these hydrogen bonds [42]. As explained to the N−H group, the peak attributed to hydrogen bonded carbonyl group shows a decline in intensity and moves from 1637 cm^{-1} to 1641 cm^{-1}, for the same reason. Furthermore, a great reduction in O−H broad peak intensity at 3400-3700 cm^{-1} is observed, compared to neat the PEBAX spectra of Fig. 2 (d) [17,40].

Fig. 2 (f) shows the FTIR spectra of nanocomposite membrane incorporating the amine functionalized silica nanoparticles. As explained before, the NH_2 group of nanoparticles surface is not directly recognizable in the spectra of the nanocomposite membranes due to the presence of abundant OH groups in the same region of frequencies, but there is another extra peak of aliphatic amine related to the presence of amine functionalized nanoparticles at around 2900 cm^{-1}, in the spectrum of the PEBAX/AFS 15% membrane. One observes that the broad peak corresponding to O−H bond increases in intensity compared to the non-functionalized nanocomposite membrane spectra as presented in Fig. 2 (e). It is also observed that the two peaks related to the N−H group show an increment in intensity, and the peak at 3202 cm^{-1} is moved right to lower frequencies. Based on the mentioned changes in the spectra, it is concluded that interactions between the amine functionalized nanoparticles and polymer chains are through intermolecular hydrogen bonding between the amine terminals of functionalized silica nanoparticles and ether oxygen atoms of the soft segment or amide nitrogen of PA segments [41,43,44].

3.1.2. FESEM observations

In general, separation properties of membranes mainly depend on their structure and morphology of the finally prepared films [45,46]. Fig. 3(a–h) shows a comparison between FESEM cross-section images of the nanocomposite membranes fabricated by the pristine and the amine functionalized silica nanoparticles. The considerable point to discuss about, is the effects of loading of silica and amine functionalized silica nanoparticles on their dispersion and agglomeration in the polymer matrix. As illustrated, all the images reveal defect-free sections without any micro pores inside, and show dense nature of thin films.

As seen in Fig. 3(a–f), in the cross view of 5–15 wt % loaded membranes (for both S and AFS samples), silica nanoparticles are well-dispersed and no bulky agglomeration is observed. As a

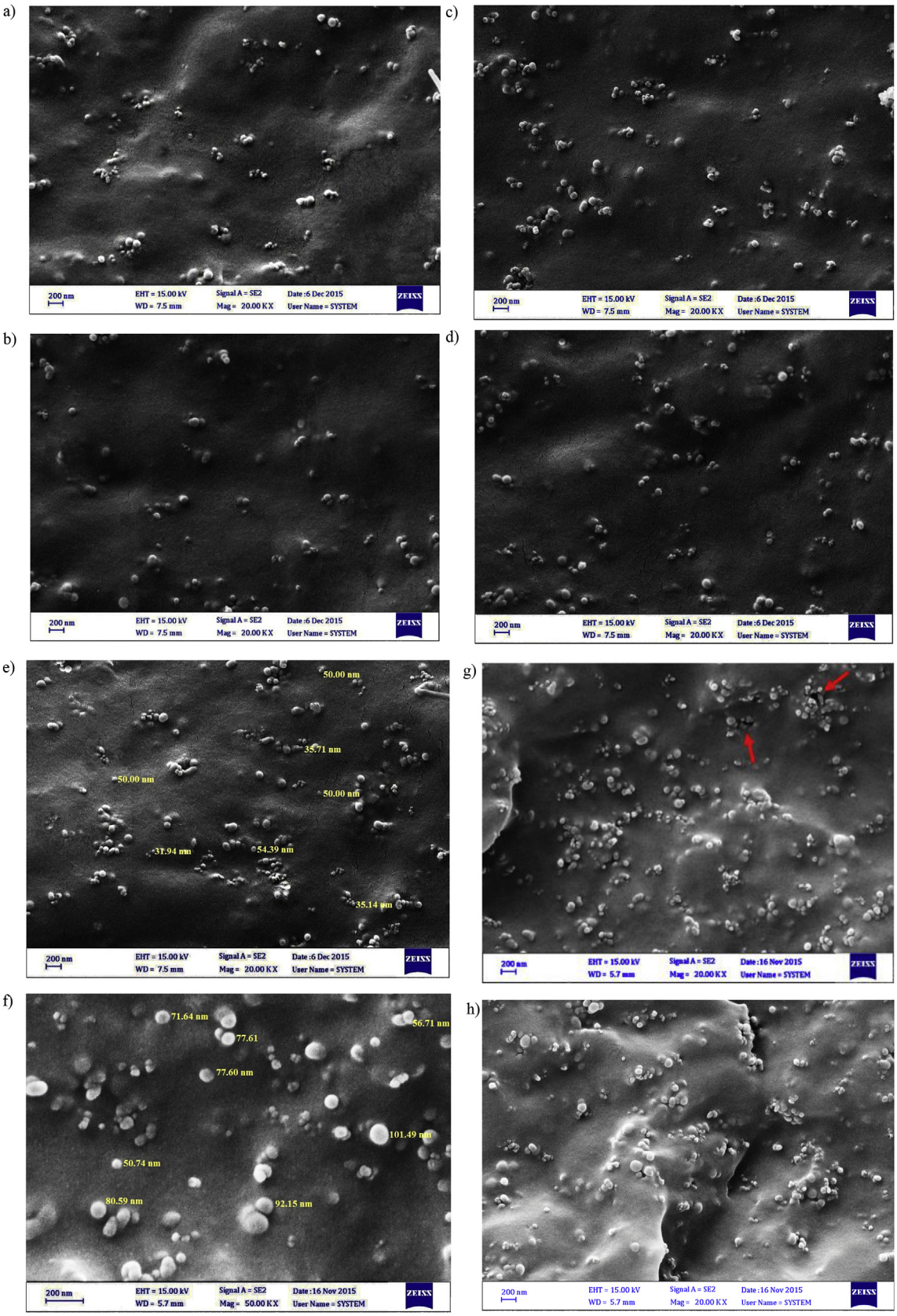

Fig. 3. FESEM images of the cross-section view of a) PEBAX/S-5, b) PEBAX/AFS-5, c) PEBAX/S-10, d) PEBAX/AFS-10, e) PEBAX/S-15, f) PEBAX/AFS-15, g) PEBAX/S-20 and h) PEBAX/AFS-20 membranes.

matter of fact, the silica nanoparticles tendency for agglomeration and sedimentation in the S-X membranes is negligible due to the applied high-power sonication. Furthermore, the amine functionalized silica nanoparticles are well-dispersed and no clustered agglomeration is seen because of the applied high-power sonication and tendency of amine sites to interact with amide groups of the polymer chains through hydrogen bonding due to the high basicity of amine functional groups, which avoids formation of unwanted voids at the interface. The FTIR analysis also showed these interactions between the polymer and the nanoparticles, clearly. However, Fig. 3 (g and h) shows that at the maximum loading of 20 wt %, compared to other loadings of the same type, some sort of agglomeration is observed and the nanoparticles tend to get closer to each other. In fact, by increasing the nanoparticles loading, their dispersion in the polymer matrix goes toward appearing more flecks, agglomerations and sedimentation and as a consequence, this may lead to the formation of non-selective voids, as assigned in Fig. 3 (g). These voids are expected to have unwanted negative effects on the membranes separation performance [41,47].

In the FESEM images as seen in Fig. 3 (e, f), it is also observed that compared to the neat silica nanoparticles, the functionalized single nanoparticles are larger in average diameter due to the formation of new layers of grafted chains of propylamine on their surface [48].

3.1.3. XRD analysis

X-ray diffraction patterns of the S and AFS nanoparticles, neat PEBAX and the nanocomposite membranes are displayed in Fig. 4. The S and AFS nanoparticles patterns consist of wide broad peaks at the center of $2\theta = 21^{\circ}$, which confirms their mostly amorphous nature [49]. As illustrated, the peak positions and intensities for the AFS nanoparticles are similar with the neat silica nanoparticles pattern. The almost unchanged silica nanoparticles pattern after the functionalization process (including cross linking of the grafted propylamine chains on the surface and formation of a 3-dimensional lattice around it) in comparison with the neat silica nanoparticles, shows that grafting occurs with no detectable changes in the crystalline structure of neat silica nanoparticles [50–52]. XRD patterns of the PEBAX membranes consist of two main diffraction peaks at around $2\theta = 12^{\circ}$ and $2\theta = 24^{\circ}$ which show the semi-crystalline structure of the polymer. The copolymer contains PE and PA segments, which form a semi-crystalline structure resulted by hydrogen bonding between the PA groups [53].

It is observed that for the nanocomposite membranes, the addition of silica nanoparticles to the polymer matrix decreases the intensity of the polymer characteristic peaks and by increasing the nanoparticles loading up to 20 wt %, this effect becomes more severe. This reveals that in the presence of nanoparticles, the total crystallinity of the membranes decreases and the amorphous phase grows up as the interchain hydrogen bonds between the polymer segments are broken, based on the FTIR results [41,54]. Moreover, it can be seen that the broad peak of nanoparticles at 21° appears noticeably in the nanocomposite patterns, as the loading goes up. Therefore, the polymer peaks pattern becomes marginally broader. Further investigations of the diffractograms showed that by increasing the loading from 5 to 20 wt %, the characteristic peak of polymer slightly shifts to lower degrees from 24.6° to 23.06°, corresponding to the increased d-spacing parameter of the polymer chains from 3.61 to 3.87 Å. This suggests an increase in intersegmental spacing of polymer chains, leading to higher fractional free volume (FFV) and more amorphous nature of the polymer [55]. Thus, gas permeabilities through the nanocomposite membranes are expected to be increased, because of the changes in polymer crystalline regions, intersegment distances and FFV [56].

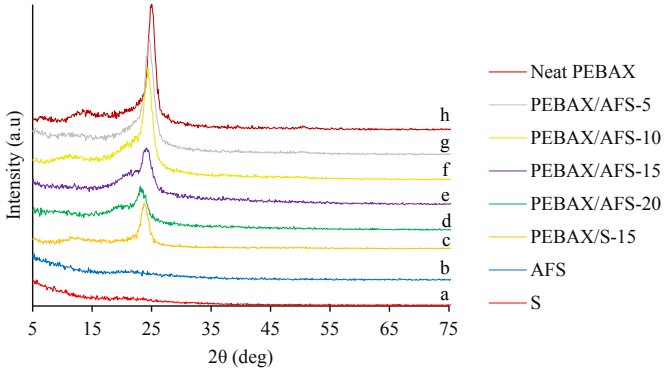

Fig. 4. X-ray diffraction patterns of a) SiO_2 and b) SiO_2-NH_2 nanoparticles and c) neat PEBAX, PEBAX/AFS-5, PEBAX/AFS-10, PEBAX/AFS-15, PEBAX/AFS-20 and PEBAX/S-15 membranes.

3.1.4. Quantification of amine sites

In addition to the FTIR spectra, functionalization of the nanoparticles was confirmed by the presence of nitrogen in the CHN elemental analysis results, as provided in Table 1. Since each nitrogen atom represents one amine functional group attached to a propyl chain, the percentage of nitrogen in the analyzed AFS nanoparticles' sample gives the total number of amine sites grafted on nanoparticles surfaces, considering the point that the percentage of nitrogen in the pristine silica nanoparticles is zero regarding the manufacturer information. Using the total surface area of the AFS nanoparticles, the total number of amine sites could be calculated as 7.94 per nm^2 of nanoparticle surface, using the method reported by Hak-Sung Jung et al. [38]; However, not all the amine sites are "active" to react with CO_2 molecules, because during the functionalization process, there is a possibility for the amino propyl chains to attach undesirably to the surface, as schematically represented in Fig. 5 (2, 5). Therefore, an "amine efficiency" could be defined by comparing the total number of amine sites (7.94 n/nm^2) and the number of active sites resulting from back titration analysis (5.31 n/nm^2), as 66.8%.

3.2. Gas separation performance

3.2.1. Adsorption performance of nanoparticles

CO_2 and CH_4 adsorption isotherms for pristine and amine functionalized nanoparticles are shown in Fig. 6. The adsorption capacity of nanoparticles depends mostly on characteristics of adsorbed gas molecules and surface functional groups. For both pristine and functionalized nanoparticles, the adsorbed amount of CO_2 molecules is higher than that of CH_4 molecules, because molecules with dipole moment (i.e. CO_2) tend to interact more with functional groups compared to nonpolar molecules, such as CH_4 [57]. Consequently, the adsorbed amounts of CH_4 molecules to the nanoparticles are too low, as seen obviously. This little amount is related to symmetric vibrations, which cause temporary polarity and increase molecules tendency to interact with surface functional groups [58]. The type of this functional group is an effective parameter on gas adsorption properties of nanoparticles, as said before. Investigation of adsorption isotherms shows that CO_2 molecules are adsorbed more on amine functionalized nanoparticles in comparison with neat ones because the nucleophile reaction between gas molecules with NH_2 functional groups is considerably stronger and more effective than with OH groups [59]. Reversibility of these reactions demonstrates that CO_2 molecules can leave the surface again due to the instability of carbonate compounds. As reported by Wang et al., the gas adsorption capacity

Table 1
CHNO elemental analysis results.

Element	Weight (mg)	Weight (%)	Reten, Time (min)	Response	Carbon response ration
Nitrogen	0.092	0.93	1.217	272.301	0.166
Carbon	0.270	2.74	2.233	1641.224	1.000
Hydrogen	0.041	0.42	9.717	599.106	0.395
Total	9.848	4.09			

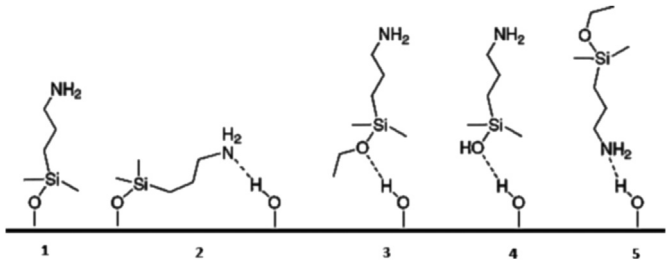

Fig. 5. Various interactions of aminosilane molecules and silica surface.

of nanoparticles is greatly affected by gas temperature and pressure and declines considerably with increasing temperature [59,60]. Accordingly, to assure the complete desorption of gas molecules from the surface of nanoparticles for further applications, this process is facilitated using vacuum and thermal treatments. The adsorption isotherms of Fig. 6 also indicate that with increasing pressure from 3 to 10 bar, CO_2 adsorption capacity increases for both nanoparticles. The amount of adsorbed CO_2 of pristine nanoparticles is 0.01 mmol/g at 3 bar and reaches 0.03 mmol/g as pressure increases to 10 bar, whereas these amounts of amine functionalized nanoparticles evidently increase after amine modification so that CO_2 adsorption capacity increases sharply from 0.02 mmol/g to 0.09 mmol/g. In both isotherms, a slight increase in adsorption capacity of CO_2 for pressure change from 9 to 10 bar shows that they are getting to reach constant amounts, and the equilibrium adsorption capacities are obtained [60–62]. The results reveal that amine functionalization effectively enhances the CO_2 adsorption capacity of pristine nanoparticles and increases their selective adsorption towards CH_4 molecules.

3.2.2. *Effect of nanoparticles loading*

Effect of nanoparticles loading on the permeability of the pure gases (CO_2 and CH_4) through the S-X and AFS-X nanocomposite membranes at 5 bar and 298 K is presented in Fig. 7. It is observed that by increasing the loading from 0 to 10 wt %, CO_2 permeability increases and then decreases from 10 to 20 wt %. i.e. for the S-X membranes, CO_2 permeability increases from 111.54 to 154.01 Barrer when the nanoparticles loading increases from 0 to 10 wt % and decreases to 102.14 Barrer by increasing the nanoparticles loading to 20 wt %. In lower amounts of loading (less than 10 wt %), gas permeability increases due to increasing the polymer FFV, d-spacing and chain mobility (amorphous region) by the presence of nanoparticles, as confirmed by the XRD and FTIR results, and also due to more interactions between CO_2 molecules and −OH groups of the nanoparticles surface [17]. As the nanoparticles loading passes 10 wt %, a considerable decrease in gas permeabilities is observed and this can be due to the high amounts of non-permeable nanoparticles that block the gas diffusion paths and increase tortuosity of the permeation paths [26]. It means that at higher loadings, the effect of paths blocking is dominant compared to the increased FFV and intersegment spacing. Comparison of permeation results for the S-X and AFS-X nanocomposite membranes shows significant improvement of CO_2 permeability for the AFS-X membranes, considering the point that permeation trends are similar for the both S-X and AFS-X membranes. The improvement percentage increases as the loading reach 20 wt %, i.e. increasing CO_2 permeability at 5 wt % nanoparticles loading is about 8%, while at 20 wt % this reaches 22%. The reason for this effect is that at a constant pressure, by increasing the nanoparticles loading, the total number of amine sites to interact with CO_2 molecules increases effectively, and this increases the membrane solubility leading to the higher CO_2 permeability compared to the silanol groups of the same content [22]. The reactive amine functional groups with electron donating nitrogen act as a Lewis base in front of CO_2 molecules [59]. The reactions between active amine sites and CO_2 molecules are as follows:

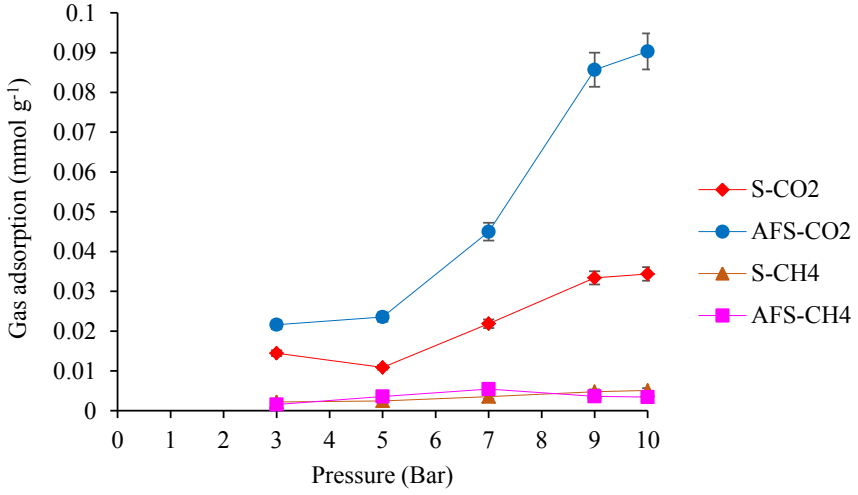

Fig. 6. CO_2 and CH_4 adsorption isotherms for pristine and amine functionalized nanoparticles.

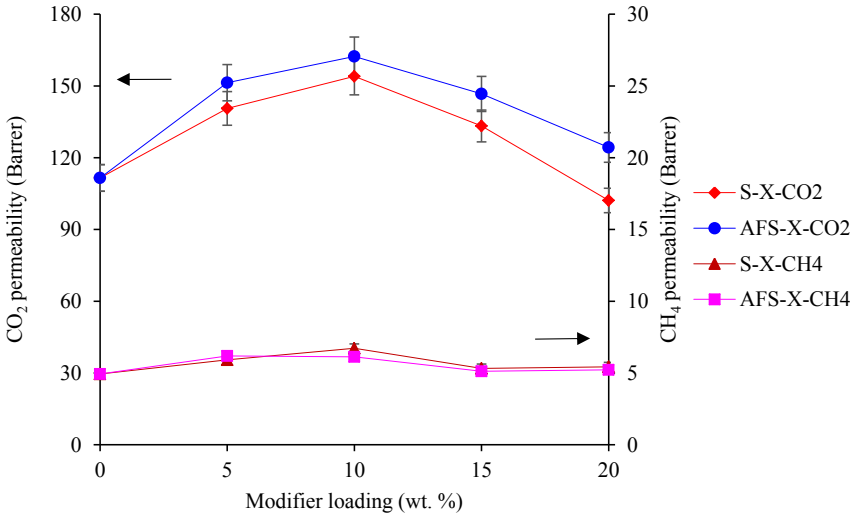

Fig. 7. The variation of CO_2 and CH_4 permeabilities with modifier loading wt. % for S-X and AFS-X membranes.

$$CO_2 + RNH_2 \leftrightarrow RNH_2^+ COO^- \quad (3)$$

$$RNH_2 + COO^- + RNH_2 \leftrightarrow RNH_3^+ + RNHCOO^- \quad (4)$$

In which a CO_2 molecule first reacts with a propylamine group and produces carbamic acid, and this product then reacts with another free amine group and results in a carbamate molecule and RNH_3^+ [60,63]. As the reactions are reversible and carbonate compounds are unstable, the molecules of CO_2 may desorb completely and regenerate the surface of nanoparticles.

This behavior is not observed for CH_4 permeability because this non-polar gas has no considerable interaction with OH and NH_2 groups. Since the kinetic diameter of this molecule is bigger, and its diffusion rate is less through the polymer matrix, the changes in permeabilities follow a mild trend, as observed on the figure. Based on these explanations, the CO_2/CH_4 ideal selectivity of the membranes increases by increasing the nanoparticles loading up to 15 wt %, and then decrease in 20 wt % as shown in Fig. 8. The reason behind this behavior is that at higher loadings, the nanoparticles agglomerate undesirably, leading towards the formation of non-selective voids, as assigned in the FESEM images in Fig. 3 (g, h). Therefore, the permeability of CH_4 slightly increases, as the voids' dimensions are comparable to the diameter of penetrant molecules. This fact was also confirmed by the XRD analysis results, which showed that by increasing the nanoparticles loading to 20 wt %, the intersegment spacing of polymer reaches 3.87 Å which is greater than the value of the CH_4 kinetic diameter (3.8 Å) and this facilitates its diffusion through the membrane. It is also observed that the reduction in ideal selectivity for the S-20 nanocomposite membrane is greater than that for the AFS-20, because neat nanoparticles have less adherence to the polymer matrix and tend to form bulk agglomerates, leading to formation of more voids in the polymer-modifier interface and non-selective channels between agglomerates, while the AFS nanoparticles are more compatible with the polymer matrix and have fewer defects.

3.2.3. Effect of pressure

Figs. 9 and 10 show the effect of upstream pressure on permeability and ideal selectivity results of the nanocomposite membranes, respectively. Generally, by increasing pressure from 2 to 10 bar, CO_2 permeability exhibits a decrease-increase trend. In rubbery polymers, since the solubility coefficient depends on gas

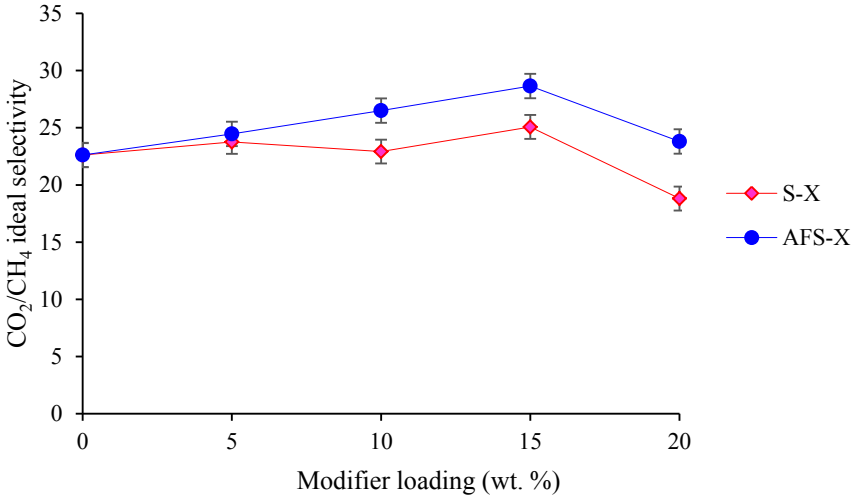

Fig. 8. The variation of CO_2/CH_4 ideal selectivity with modifier loading wt. % for S-X and AFS-X membranes.

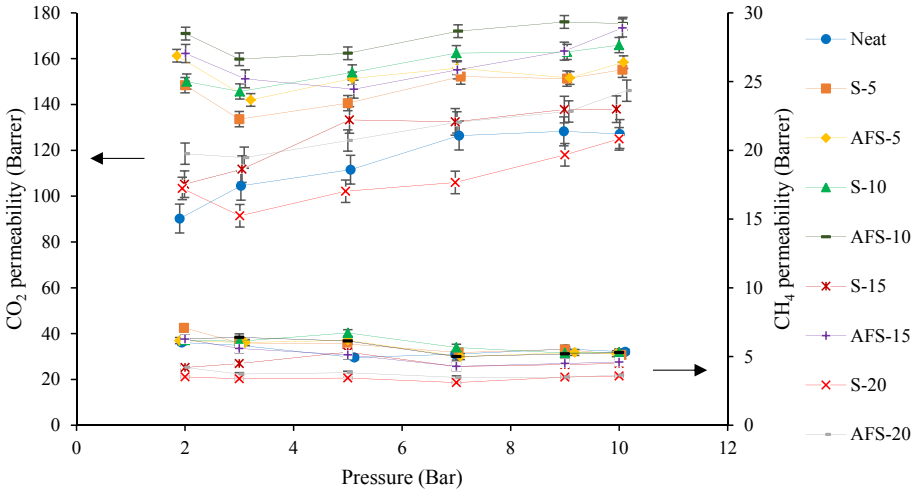

Fig. 9. The variation of CO_2 and CH_4 permeabilities with upstream pressure for S-X and AFS-X membranes.

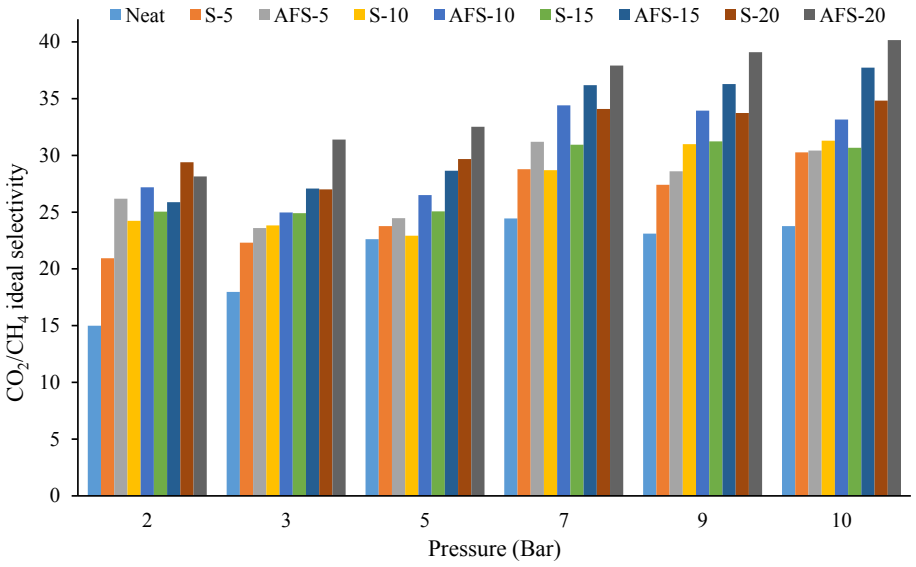

Fig. 10. The variation of CO_2/CH_4 ideal selectivity with upstream pressure for S-X and AFS-X membranes.

condensability, CO_2 molecules sorb into the polymer and plasticize it. The CO_2 sorption and plasticization increases the segmental packing, chain spacing and chain mobility so that the diffusion coefficient increases and affects gas permeability by increasing the pressure [64–66]. As reported by Bondar et al., carbon dioxide solubility in PEBAX is about 30–160 times higher than that of CH_4, and it possibly plasticizes the polymer. In pressures higher than 3 bar CO_2 permeability increases due to the polymer plasticization by CO_2 molecules [67]. As the permeability coefficients of low-sorbing penetrants are independent of pressure, the polymer matrix is not plasticized by CH_4 [68]. Therefore, due to the low solubility of CH_4 molecules into the polymer and its negligible interactions with the polymer chains, its permeability is assumed constant, compared to CO_2. Considering these explanations, CO_2/CH_4 ideal selectivity exhibits an increasing trend by increasing the pressure from 2 to 10 bar. i.e. for the neat PEBAX membrane the ideal selectivity with a 58% increase, reaches from 14.99 at 2 bar to 23.77 at 10 bar. These values are a little different for other nanocomposite membranes so that for the AFS-20 membrane, a 42% increase in ideal selectivity from 28.14 to 40.16 is observed. This reduction in the amount of ideal selectivity improvement with pressure, is due to the fact that compared to the neat membrane, nanocomposite membranes have a lower capacity of CO_2 sorption and chain mobility caused by the presence of impermeable nanoparticle.

3.2.4. *Effect of temperature*

Figs. 11 and 12 Show effects of temperature on permeability and ideal selectivity of the S-10 nanocomposite membrane at 5 bar. By increasing temperature, the CO_2/CH_4 ideal selectivity declines significantly, i.e. at the constant pressure of 5 bar with increasing operating temperature from 25 to 75 °C, the CO_2 permeability increases by nearly 60%, from 129.60 to 205.10 Barrer and the CH_4's changes from 5.64 to 16.59 Barrer, because of increasing movements of polymer chains [65]. These results lead to decrease in the ideal selectivity from 22 to 12 and show that the effect of temperature on the permeability of CH_4 is more than CO_2. The graphs of Fig. 11 shows that in a moderate temperature range, no thermal transitions in the structure of the polymer occur and therefore, the permeabilities change linearly with the temperature [69,70]. As

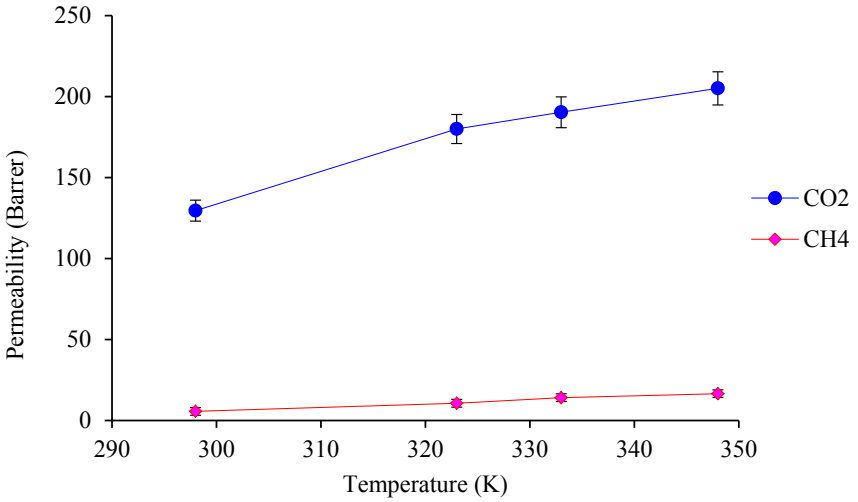

Fig. 11. The variation of CO_2 and CH_4 permeabilities with feed temperature for S-10 membrane.

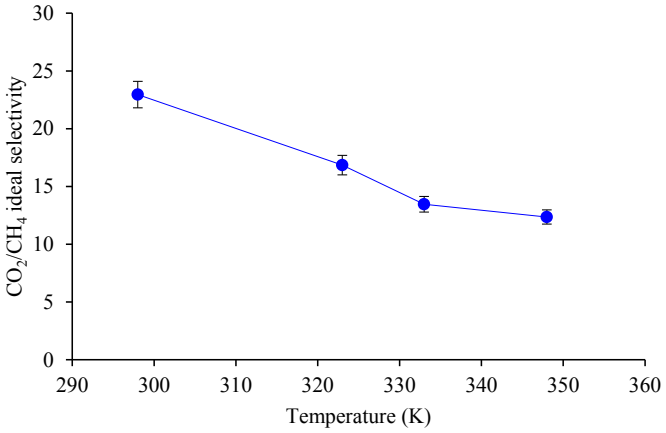

Fig. 12. The variation of CO_2/CH_4 ideal selectivity with feed temperature for S-10 membrane.

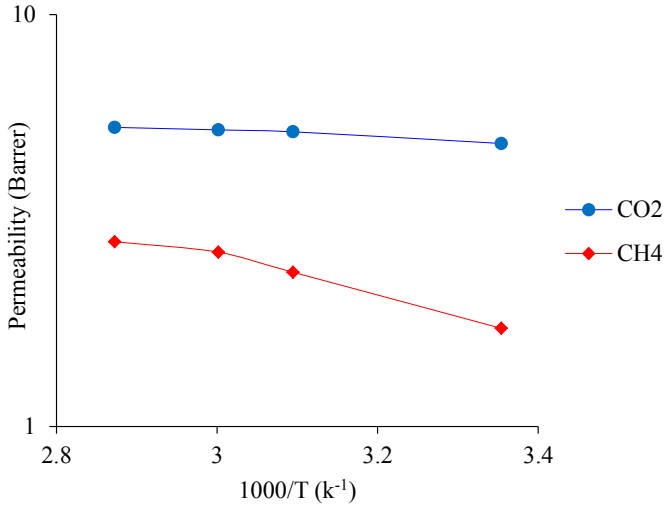

Fig. 13. Linear-logarithmic functionality of CO_2 and CH_4 permeabilities vs. feed temperature at 5 bar.

reported by Qipeng et al. due to melting temperature of PEO segments (about 50 °C), gas permeabilities through the polymer are strongly temperature dependent [71]. The reason for the significant decrease in CO_2/CH_4 ideal selectivity can be explained based on reducing solubility selectivity more significantly than diffusion selectivity [59]. Their temperature dependency is described using Eq. (5) and Eq. (6):

$$D = D_0 \exp\left(\frac{-E_d}{RT}\right) \tag{5}$$

$$S = S_0 \exp\left(\frac{-\Delta H_s}{RT}\right) \tag{6}$$

In which E_d and ΔH_s are activation energy of diffusion and heat of sorption, respectively [19].

For a better explanation to this effect, the temperature-dependency of penetrants through the dense polymer was also investigated by the Van't Hoff–Arrhenius equation, which is shown in a semi-logarithmic graph in Fig. 13.

$$P = P_0 \exp\left(\frac{-E_p}{RT}\right) \tag{7}$$

In the above equation, P_0 is the pre-exponential factor (Barrer), R is the gas constant, T is temperature (K) and E_p is the apparent activation energy of permeation (J/mol). From the slopes of *Ln P* versus $1000/T$ graphs (Fig. 13), the activation energy values for CH_4 and CO_2 gases can be obtained as 59.82 and 25.14 J/mol, respectively. This confirms the temperature sensitivity of low-permeable gases (CH_4) and describes that at lower temperatures, the membranes have better performance due to higher sorption of CO_2, compared to elevated temperatures [72].

3.3. Results comparison with the Robeson diagram

In order to investigate the effect of surface modification of nanoparticles and their interactions with CO_2 and CH_4 molecules on gas separation properties of the membranes and compare the performance of nanocomposite membranes in the current work with the Robeson upper bound, the data points were located on the selectivity-permeability plot (Robeson diagram). The main purpose of most research activities is to get closer to the Robeson upper bound or to pass the limit, which firstly presented in 1991 [73] and recently re-computed in 2008 [74]. Fig. 14 shows separation

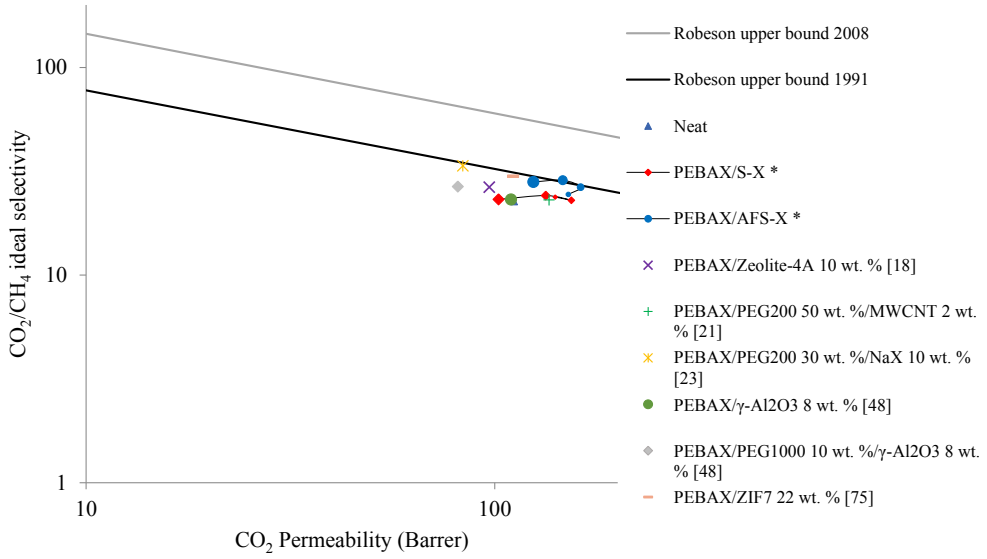

* The increase in modifiers loading of the membranes is followed by the increase in markers size.

Fig. 14. The comparison of separation performance of S-X and AFS-X membranes with the Robeson upper limit.

properties of the nanocomposite membranes of the current work with the optimum performances (S-15 and AFS-15) at temperature of 25 °C and pressure of 2 bar.

As illustrated in the figure, firstly, by increasing silica nanoparticles loading to 15 wt %, the membranes' performance enhances compared to the neat membrane, in both permeability and selectivity. Secondly, amine modification of these nanoparticles for the loadings up to 15 wt %, shifts the coordinates of corresponding data points of prepared membranes towards the Robeson upper bound. However, further increasing of the silica nanoparticles loading and the amine modification of these nanoparticles, distances data points of the prepared membranes from the Robeson upper bound. Additionally, performance of some other PEBAX1657 based nanocomposite membranes reported in the literature is shown in Fig. 14 [18,21,23,48,75]. As observed, the data point coordinates of the prepared nanocomposite membrane containing 15 wt % of AFS nanoparticles is closer to the Robeson upper bound than those of other membranes. Consequently, the prepared membranes can be considered as one of the appropriate candidates for CO_2/CH_4 separation.

4. Conclusion

Incorporation of inorganic nanoparticles into the polymeric matrix is among the recent membrane development methods to simultaneously combine the polymer's processability and flexibility and nanoparticles' selectivity and thermal and mechanical stability. In this work, nanocomposite membranes base on amino functionalized fumed silica and PEBAX 1657 were prepared. The nanoparticles and nanocomposite membranes were characterized using FESEM, FTIR, XRD and CHNO analyses. The results showed that with the aid of amine functionalization, dispersion of SiO_2-NH_2 into the polymer matrix is more uniform, and this leads to the formation of high-quality membranes. The gas separation results showed that adding the nanoparticles to the polymer matrix increases CO_2 permeability and CO_2/CH_4 ideal selectivity, simultaneously, due to the higher CO_2 adsorption capacity of nanoparticles after amine modification.

Acknowledgment

The authors wish to thank the Iran National Science Foundation (INSF) for supporting the research.

References

[1] O.G. Nik, X.Y. Chen, S. Kaliaguine, Functionalized metal organic framework-polyimide mixed matrix membranes for CO2/CH4 separation, J. Membr. Sci. 413–414 (0) (2012) 48–61.
[2] M. Peydayesh, et al., Preparation and characterization of SAPO-34 – matrimid® 5218 mixed matrix membranes for CO2/CH4 separation, Chem. Eng. Res. Des. 91 (7) (2013) 1335–1342.
[3] D.D. Iarikov, S. Ted Oyama, Chapter 5-review of CO2/CH4 separation membranes, in: S.T. Oyama, M.S.-W. Susan (Eds.), Membrane Science and Technology, Elsevier, 2011, pp. 91–115.
[4] L. Zhao, et al., Promising monolayer membranes for CO2/N2/CH4 separation: graphdiynes modified respectively with hydrogen, fluorine, and oxygen atoms, Appl. Surf. Sci. 405 (2017) 455–464.
[5] Y. Wang, et al., Theoretical investigation of gas separation in functionalized nanoporous graphene membranes, Appl. Surf. Sci. 407 (2017) 532–539.
[6] M. Semsarzadeh, et al., Structural and transport properties of polydimethylsiloxane based polyurethane/silica particles mixed matrix membranes for gas separation, Korean J. Chem. Eng. 31 (5) (2014) 841–848.
[7] J.-H. Moon, et al., Separation characteristics of tetrapropylammoniumbromide templating silica/alumina composite membrane in CO2/N2, CO2/H2 and CH4/H2 systems, Korean J. Chem. Eng. 21 (2) (2004) 477–487.
[8] M. Pakizeh, et al., Preparation and characterization of dimethyldichlorosilane modified SiO2/PSf nanocomposite membrane, Korean J. Chem. Eng. 30 (3) (2013) 751–760.
[9] A.R. Moghadassi, et al., Preparation and characterization of acrylonitrile butadiene styrene and cadmium sulfide nanoparticle mixed matrix membranes for gas separation, Asia-Pacific J. Chem. Eng. 8 (3) (2013) 311–317.
[10] R.W. Baker, Membrane Technology and Applications, John Wiley & Sons, Ltd, West Sussex, England, 2004.
[11] Y. Zhu, et al., Highly hydrogen-permselective zeolitic imidazolate framework ZIF-8 membranes prepared on coarse and macroporous tubes through repeated synthesis, Sep. Purif. Technol. 146 (2015) 68–74.
[12] X. Ren, et al., Poly (amide-6-b-ethylene oxide) multilayer composite membrane for carbon dioxide separation, Int. J. Greenh. Gas Control 8 (2012) 111–120.
[13] E.A. Feijani, H. Mahdavi, A. Tavasoli, Poly (vinylidene fluoride) based mixed matrix membranes comprising metal organic frameworks for gas separation applications, Chem. Eng. Res. Des. 96 (2015) 87–102.
[14] S.H.M.A.A. Djirsarai, Nano composite PEBAX®/PEG membranes: effect of MWNT filler on CO2/CH4 separation, Int. J. Nano Dimens. 5 (3) (2014) 247–254.
[15] Y. Feng, et al., Inorganic particle enhanced polymer hollow fiber membranes with high mechanical properties, Mater. Chem. Phys. 167 (2015) 209–218.
[16] I.M. Tkachenko, et al., Synthesis, gas transport and dielectric properties of

fluorinated poly(arylene ether)s based on decafluorobiphenyl, Mater. Chem. Phys. 183 (2016) 279–287.
[17] R.S. Murali, et al., Gas permeation behavior of Pebax-1657 nanocomposite membrane incorporated with multiwalled carbon nanotubes, Ind. Eng. Chem. Res. 49 (14) (2010) 6530–6538.
[18] R. Surya Murali, et al., Mixed matrix membranes of Pebax-1657 loaded with 4A zeolite for gaseous separations, Sep. Purif. Technol. 129 (2014) 1–8.
[19] J.H. Kim, S.Y. Ha, Y.M. Lee, Gas permeation of poly(amide-6-b-ethylene oxide) copolymer, J. Membr. Sci. 190 (2) (2001) 179–193.
[20] B. Yu, et al., Pebax-1657 nanocomposite membranes incorporated with nanoparticles/colloids/carbon nanotubes for CO2/N2 and CO2/H2 separation, J. Appl. Polym. Sci. 130 (4) (2013) 2867–2876.
[21] S. Habibzare, M. Asghari, A. Djirsarai, Nano composite PEBAX®/PEG membranes: effect of MWNT filler on CO2/CH4 separation, Int. J. Nano Dimens. 5 (Issue 3) (2014) 247–254.
[22] D. Zhao, et al., Gas separation properties of poly(amide-6-b-ethylene oxide)/amino modified multi-walled carbon nanotubes mixed matrix membranes, J. Membr. Sci. 467 (0) (2014) 41–47.
[23] A.M.M.N.V.Z.G.K.M. Asghari, Nano composite PEBAX® membranes: effect of zeolite X filler on CO2 permeation, Int. J. Nano Dimens. 5 (1) (2014) 83–89.
[24] S. Wang, et al., Pebax–PEG–MWCNT hybrid membranes with enhanced CO2 capture properties, J. Membr. Sci. 460 (2014) 62–70.
[25] Z. Ye, et al., Preparation of a novel polysulfone/polyethylene oxide/silicone rubber multilayer composite membrane for hydrogen–nitrogen separation, Mater. Chem. Phys. 94 (2) (2005) 288–291.
[26] A. Ghadimi, T. Mohammadi, N. Kasiri, A novel chemical surface modification for the fabrication of PEBA/SiO2 nanocomposite membranes to separate CO2 from syngas and natural gas streams, Ind. Eng. Chem. Res. 53 (44) (2014) 17476–17486.
[27] S. Hassanajili, M. Khademi, P. Keshavarz, Influence of various types of silica nanoparticles on permeation properties of polyurethane/silica mixed matrix membranes, J. Membr. Sci. 453 (2014) 369–383.
[28] H. Sun, et al., Cardo polyimides/TiO2 mixed matrix membranes: synthesis, characterization, and gas separation property improvement, Sep. Purif. Technol. 122 (0) (2014) 367–375.
[29] K.M. Gheimasi, et al., Prediction of CO2/CH4 permeability through sigma-1–matrimid®5218 MMMs using the maxwell model, J. Membr. Sci. 466 (0) (2014) 265–273.
[30] A.L. Ahmad, et al., A cellulose acetate/multi-walled carbon nanotube mixed matrix membrane for CO2/N2 separation, J. Membr. Sci. 451 (0) (2014) 55–66.
[31] Y. Zhang, R. Wang, Novel method for incorporating hydrophobic silica nanoparticles on polyetherimide hollow fiber membranes for CO2 absorption in a gas–liquid membrane contactor, J. Membr. Sci. 452 (0) (2014) 379–389.
[32] A.L. Khan, et al., Mixed matrix membranes comprising of Matrimid and –SO3H functionalized mesoporous MCM-41 for gas separation, J. Membr. Sci. 447 (0) (2013) 73–79.
[33] S. Sorribas, et al., Mixed matrix membranes comprising silica-(ZIF-8) core–-shell spheres with ordered meso–microporosity for natural- and bio-gas upgrading, J. Membr. Sci. 452 (0) (2014) 184–192.
[34] Hu, L., et al., Composites of Ionic Liquid and Amine-modified SAPO 34 Improve CO2 Separation of CO2-selective Polymer Membranes. Applied Surface Science.
[35] E. Bourgeat-Lami, P. Espiard, A. Guyot, Poly(ethyl acrylate) latexes encapsulating nanoparticles of silica: 1. Functionalization and dispersion of silica, Polymer 36 (23) (1995) 4385–4389.
[36] M. Iqbal, et al., Solvent effect on morphology and CO2/CH4 separation performance of asymmetric polycarbonate membranes, J. Membr. Sci. 318 (1–2) (2008) 167–175.
[37] M. Isanejad, N. Azizi, T. Mohammadi, Pebax membrane for CO2/CH4 separation: effects of various solvents on morphology and performance, J. Appl. Polym. Sci. 134 (9) (March 5, 2017).
[38] H.-S. Jung, D.-S. Moon, J.-K. Lee, Quantitative analysis and efficient surface modification of silica nanoparticles, J. Nanomater. 2012 (2012) 8.
[39] A. D'Agostino, et al., Development of nanocomposite based on hydroxyethylmethacrylate and functionalized fumed silica: mechanical, chemico–physical and biological characterization, J. Mater. Sci. Mater. Med. 22 (3) (2011) 481–490.
[40] H. Rabiee, A. Ghadimi, T. Mohammadi, Gas transport properties of reverse-selective poly (ether-b-amide6)/[Emim][BF 4] gel membranes for CO 2/light gases separation, J. Membr. Sci. 476 (2015) 286–302.
[41] N.L. Le, Y. Wang, T.-S. Chung, Pebax/POSS mixed matrix membranes for ethanol recovery from aqueous solutions via pervaporation, J. Membr. Sci. 379 (1) (2011) 174–183.
[42] J.H. Kim, Y.M. Lee, Gas permeation properties of poly (amide-6-b-ethylene oxide)–silica hybrid membranes, J. Membr. Sci. 193 (2) (2001) 209–225.
[43] C. Sequeira, D. Santos, Polymer Electrolytes: Fundamentals and Applications, Elsevier, 2010.
[44] J. McMurry, Organic Chemistry, Cengage Learning, Boston, MA, 2016.
[45] J.K. Adewole, et al., Comparative studies on the effects of casting solvent on physico-chemical and gas transport properties of dense polysulfone membrane used for CO2/CH4 separation, J. Appl. Polym. Sci. 132 (27) (2015).
[46] P. Luis, D. Van Aubel, B. Van der Bruggen, Technical viability and exergy analysis of membrane crystallization: closing the loop of CO 2 sequestration, Int. J. Greenh. Gas Control 12 (2013) 450–459.
[47] P. Rani, R. Srivastava, Nucleophilic addition of amines, alcohols, and thiophenol with epoxide/olefin using highly efficient zirconium metal organic framework heterogeneous catalyst, RSC Adv. 5 (36) (2015) 28270–28280.
[48] H.R. Mahdavi, N. Azizi, T. Mohammadi, Performance evaluation of a synthesized and characterized Pebax1657/PEG1000/γ-Al2O3 membrane for CO2/CH4 separation using response surface methodology, J. Polym. Res. 24 (5) (2017) 67.
[49] S. Azarshin, J. Moghadasi, Z.A. aboosadi, Surface functionalization of silica nanoparticles to improve the performance of water flooding in oil wet reservoirs, Energy Explor. Exploitation 35 (6) (2017) 685–697, 0144598717716281.
[50] C.P. Cabello, et al., Enhanced CO2 adsorption capacity of amine-functionalized MIL-100(Cr) metal-organic frameworks, CrystEngComm 17 (2) (2015) 430–437.
[51] M. Jafarzadeh, I. Rahman, C. Sipaut, Optical properties of amorphous organo-modified silica nanoparticles produced via co-condensation method, Ceram. Int. 36 (1) (2010) 333–338.
[52] G. Bayramoglu, et al., Removal of metal complexed azo dyes from aqueous solution using tris (2-aminoethyl) amine ligand modified magnetic p (GMA-EGDMA) cationic resin: adsorption, isotherm and kinetic studies, Chem. Eng. Res. Des. 124 (August 2017) 85–97.
[53] H. Nagar, et al., Air separation by facilitated transport of oxygen through a Pebax membrane incorporated with a cobalt complex, RSC Adv. 5 (93) (2015) 76190–76201.
[54] R. Hodge, G.H. Edward, G.P. Simon, Water absorption and states of water in semicrystalline poly (vinyl alcohol) films, Polymer 37 (8) (1996) 1371–1376.
[55] R.S. Murali, et al., Nanosilica and H-Mordenite incorporated Poly (ether-block-amide)-1657 membranes for gaseous separations, Microporous Mesoporous Mater. 197 (2014) 291–298.
[56] S. Araki, et al., Preparation and CO 2 adsorption properties of aminopropyl-functionalized mesoporous silica microspheres, J. colloid interface Sci. 339 (2) (2009) 382–389.
[57] P. Chowdhury, et al., Adsorption of CO, CO 2 and CH 4 on Cu-BTC and MIL-101 metal organic frameworks: effect of open metal sites and adsorbate polarity, Microporous Mesoporous Mater. 152 (2012) 246–252.
[58] P. Serra-Crespo, et al., Synthesis and characterization of an amino functionalized MIL-101 (Al): separation and catalytic properties, Chem. Mater. 23 (10) (2011) 2565–2572.
[59] S. Shishatskiy, et al., Quaternary ammonium membrane materials for CO 2 separation, J. Membr. Sci. 359 (1) (2010) 44–53.
[60] L. Wang, et al., CO2 adsorption on SBA-15 modified by aminosilane, Chin. J. Catal. 28 (9) (2007) 805–810.
[61] J. Duan, et al., High CO 2/N 2/O 2/CO separation in a chemically robust porous coordination polymer with low binding energy, Chem. Sci. 5 (2) (2014) 660–666.
[62] V. Zeleňák, et al., Amine-modified ordered mesoporous silica: effect of pore size on carbon dioxide capture, Chem. Eng. J. 144 (2) (2008) 336–342.
[63] Sanz, R., et al., H2 production via water gas shift in a composite Pd membrane reactor prepared by the pore-plating method. International Journal of Hydrogen Energy, (0).
[64] N.N. Li, Plasticizing effect of permeates on the selectivity of polymeric membranes, Ind. Eng. Chem. Prod. Res. Dev. 8 (3) (1969) 281–286.
[65] A. Car, et al., Pebax®/polyethylene glycol blend thin film composite membranes for CO 2 separation: performance with mixed gases, Sep. Purif. Technol. 62 (1) (2008) 110–117.
[66] V. Bondar, B. Freeman, I. Pinnau, Gas transport properties of poly (ether-b-amide) segmented block copolymers, J. Polym. Sci. Part B Polym. Phys. 38 (15) (2000) 2051–2062.
[67] S.R. Reijerkerk, et al., On the effects of plasticization in CO 2/light gas separation using polymeric solubility selective membranes, J. Membr. Sci. 367 (1) (2011) 33–44.
[68] P. Pfromm, in: Y. Yampolskii, I. Pinnau, B.D. Freeman (Eds.), Materials Science of Membranes for Gas and Vapour Separation, Wiley, 2006.
[69] K.-i. Okamoto, et al., Gas permeation properties of poly (ether imide) segmented copolymers, Macromolecules 28 (20) (1995) 6950–6956.
[70] J. Li, et al., Effect of polyethyleneglycol (PEG) on gas permeabilities and permselectivities in its cellulose acetate (CA) blend membranes, J. Membr. Sci. 138 (2) (1998) 143–152.
[71] G. Qipeng, X. Hechang, M. Dezhu, Effect of temperature on gas permeation of polymer blends. I. Poly (ethylene oxide)/copolyester–polyurethane, J. Appl. Polym. Sci. 39 (11–12) (1990) 2321–2330.
[72] L. Liu, A. Chakma, X. Feng, CO2/N2 separation by poly (ether block amide) thin film hollow fiber composite membranes, Ind. Eng. Chem. Res. 44 (17) (2005) 6874–6882.
[73] L.M. Robeson, Correlation of separation factor versus permeability for polymeric membranes, J. Membr. Sci. 62 (2) (1991) 165–185.
[74] L.M. Robeson, The upper bound revisited, J. Membr. Sci. 320 (1–2) (2008) 390–400.
[75] T. Li, et al., Carbon dioxide selective mixed matrix composite membrane containing ZIF-7 nano-fillers, J. Membr. Sci. 425 (2013) 235–242.